Semnan University

Mechanics of Advanced Composite Structures

Journal homepage: https://macs.semnan.ac.ir/

ISSN: 2423-7043

Research Article

Performance Evaluation of Epoxy-Based Smart Composite with Integrated Touch Sensor

Mohan Kumar T S [a*]

(Mohan Kumar T S [a*])

[a] *Department of Industrial Engineering and Management, Siddaganga Institute of Technology, Tumkur, 572103, India*

ARTICLE INFO

Article history:

Received: 2024-10-19
Revised: 2025-03-22
Accepted: 2025-05-12

Keywords:

Smart Composite;
Capacitive Touch Sensors;
Capacitance variation;
Sensitivity;

ABSTRACT

Composite materials provide mechanical and electrical stability across diverse environmental conditions, thereby enhancing sensor durability. This study aims to fabricate novel epoxy-embedded capacitive touch sensors, Type A (Touch sensor embedded) and Type B (embedded sensor with wire loop) configurations, and test them experimentally and compare their electrical and functional characteristics. Electrical characteristics are tested using neat epoxy as a reference, and the results indicate that the progressive decrease in resistivity from pure epoxy to Type B clearly demonstrates the role of sensor configuration in enhancing electrical performance. The functional characteristics were tested based on sensing behaviors and long-term durability. The results indicate that Type A exhibits enhanced touch sensitivity, with greater capacitance variation (ΔC) and a shorter response time. Type B provides better electrical stability and dielectric damping, resulting in increased SNR (signal-to-noise ratio), enhanced repeatability, more effective resistance to noise, and lower hysteresis. Frequency-dependent dielectrics showed consistent permittivity behavior, with capacitance variations decreasing at higher frequencies. Response time and ΔC varied significantly, according to the two-sample t-tests ($p < 0.05$). For long-term aging and error analysis, less variation in measurement (less than 6%) and a coefficient of variation of around 2% were observed.

1. Introduction

Epoxy is a high-performance thermosetting polymer produced by combining an epoxy resin and a hardener (curing agent). When these two components are mixed, an exothermic cross-linking reaction occurs, transforming the liquid combination into a solid that is strong, durable, and rigid. The excellent bonding strength, chemical resistance, water resistance, and dimensional stability of this cured material are widely recognized. This cured composite is renowned for its excellent dimensional stability, water resistance, chemical resistance, and bonding strength. Many industries, including construction, aerospace, marine, automotive, electrical, and even the creative arts, employ epoxy extensively. One of its main applications is bonding strength, which may join a variety of materials, such as composites, metals, ceramics, plastics, and wood [1]. The demand for polymer composite materials continues to increase as technologies such as AI (artificial intelligence) and soft robotics advance. For efficient sensor development, CPCs (conductive polymer composites) should be able to build a sustainable

* **Corresponding author.**
E-mail address: mohammadi@gmail.com

Cite this article as:
Mohammadi, A. and Mahdi-Nia, M., 2027. Title of article. *Mechanics of Advanced Composite Structures*, 14(1), pp. xxx-xxx.
https://doi.org/10.22075/MACS.2025.39313.2050

network for data transfer, communicate smartly with their environment, and sense a wide range of external stimulation. Flexi piezoresistive pressure sensors outperform piezoelectric and capacitive sensors in sensitivity, sensing range, and signal acquisition and transformation [2]. Therefore, investigators are increasingly employing elastic and flexible materials for developing actuators, sensors, circuit boards, and other electronic parts. The tendency in electronic gadgets has been to optimize both size and performance. Flexible devices must adjust to many surfaces, whether they are flat, curved, stiff, soft, stationary, or mobile. To enable the development of new intelligent products, such as wearables and folding smartphones, the display, which is the visual output device for many electrical gadgets, has also been made more flexible [3, 4]. Flexible displays are better than their rigid counterparts in a number of aspects, such as their thinness, durability, surface parameters, and low weight [5]. To reduce size, an electronic device with a flexible screen might be folded or wrapped. To satisfy the demands of the interactions between humans and machines on these instruments, touch technology is crucial. Touch sensors that are flexible and transparent are crucial input devices for flexible displays. Usually, a display can be topped with a touch panel made up of touch sensors. By using one or more hands to touch the panel, users can enter data [6]. The touchscreen eliminates the need for input devices like a touchpad, mouse, etc., by enabling direct interaction with the displayed material. Touch screens are commonly utilized in a wide range of products, including computers, video games, mobile phones, tablets, and mall information kiosks, to provide customers with accurate, speedy, and simple interactions. While touch sensing can be accomplished in many ways, Surface acoustic wave, infrared, resistive, and capacitive technologies are commonly employed [7]. The popular capacitive touch sensors for rigid electronics are composed of a dielectric and a pair of electrode layers. These days, most flexible touch devices used are capacitive. The composition and construction of flexible touch sensors are subject to new standards. The display and touch components are separated by the out-cell layout found in traditional touchscreen laminates. This technique is inappropriate for flexible displays since it reduces flexibility by making the display heavier and thicker. Integrated touch sensors, in which part or all of the touch sensor is incorporated within the display unit, have been suggested as a way to minimize the device's overall thickness. Because of its excellent multi-touch capability and sensitivity, capacitive touch sensor technology is widely used in mobiles, smart watches, and laptops [8].

A capacitive touch sensor is made by sputtering, evaporating, and patterning a number of layers of transparent conductors onto a layer of glass. Applying AC (alternating current) to the conducting electrode causes the capacitor to become conductive. A shift in capacitance occurs when a human finger or stylus touches the sensor, disrupting the electric field. The electrode parameters, which typically vary in capacitance, might be used to locate the contact. The data is subsequently processed by a controller IC. Two distinct categories of capacitive sensing technologies are SCTS (surface capacitive touch sensing) [8] and PCTS (projected capacitive touch sensing). In addition, the two types of projected capacitive touch sensing are mutual capacitive touch and self-capacitive touch.

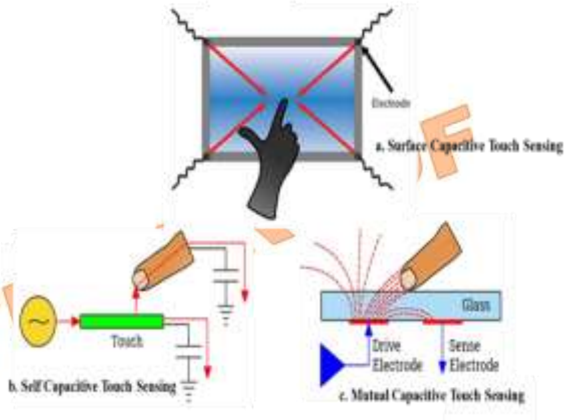

Fig. 1. Capacitive touch screen mechanisms [10].

SCTS Technique has a conducting layer on just one side of the surface of the capacitive sensor's insulating layer [9]. All four edges are linked to four synchronous AC power pulses. The AC produces a voltage field around the four edges of the touch panel surface, as illustrated in Fig. 1(a). The position of the touch can be determined through assessing the capacitance shift at all the edges. Compared to traditional resistive tactile sensing, SCTS offers many benefits, such as a harder surface, greater sensitivity, a longer lifespan, and better transmission of light. Among its many drawbacks, low resolution and incompatibility with multi-touch are the most common. Nowadays, interactive systems like touchscreen kiosks are the primary applications for it [10]. PCTS technology usually employs a number of levels of tailored electrode structures, compared to SCTS, which uses a single conductor electrode [11]. Fig. 1(b) and (c) illustrate that patterned electrodes make up the proposed capacitive touch technology [12]. Touching the sensor alters the electric field, affecting the capacitance associated with the electrode or the capacitance across subsequent electrodes [10]. The point of contact can be found using the electrode indices where capacitances vary. The projected capacitive touch sensing technology enhances human-computer interaction by supporting multi-touch, two-point touch, or pinch. Projected capacitive touch technologies can be classified as either mutual capacitive touch sensing or self-capacitive touch sensing based on how they are detected. The industry of flexible electronic devices has also entered a new phase as artificial intelligence steadily makes its way into thousands of household appliances [13]. The immense demand for electronic windows and the Internet of Things sector, along with the quick advancement of visualization technology, has raised the demand for flexible pressure sensors [14]. These demands include excellent performance, flexibility, lightweight design, and mass production, among other requirements. Conventional metal/ceramic sensors are subject to a limited sensing range and inflexible and stiff materials [15-17]. Stretchable and implantable devices for the human body may be enabled by a Polymeric composite with high stretchability. Based on the method they operate, flexible pressure sensors are divided into piezoresistive [18], capacitance [19], triboelectric, and piezoelectric [20]. Capacitance and Piezoresistive sensors have been well investigated in comparison to piezoelectric and triboelectric sensors, and it is simple to observe numerous parallels in their behavior [21], [22]. Additionally, their production techniques and operating principles are generally simple and could respond significantly better to static stimuli. The range of application could widen in the future. The obvious benefits of triboelectric and piezoelectric sensors are that they are more susceptible to dynamic stimuli and do not require an external power supply [23]. Piezoelectric layers are added to composite structures to harness sustainable vibration energy [24-26]. These layers have the ability to transform pressure, deformation, and mechanical vibrations into electrical impulses. In low-power devices like wireless sensors, this characteristic produces electricity. Piezoelectrics are used in many sensors, especially those that measure pressure, vibration, and sound, because of their sensitivity to physical changes [27], [28]. The creation of the sensor and the mounting methods used to connect it with the supporting structure are crucial to achieving a reliable structural health monitoring (SHM) of the composite. Because surface mounting is easier to install, disassemble, replace, and maintain than embedded mounting, it is the more popular of the two major mounting techniques. Even though the sensors are adhered to the composite's surface, they might be subjected to a hostile environment. As a result, it is subject to failure due to external impact and chemical corrosion. Similarly, it can be challenging to mount sensors to precisely curved surfaces, and they can easily come loose in harsh environments and after extended durations of operation. Another important issue contributing to inaccurate sensing and measurement is the relative mobility of the sensor and the analyzed part [29, 30]. Whereas embedded and surface installation in composite materials protects wiring and sensors [31], this means that the harsh environment has considerably less impact on the stability and lifespan of the sensor. Additionally, the embedded sensor is more robust than surface installation during the extended observation phase, as it is in direct contact with the structure. As a result, SHM in composites has focused on sensor functional integration. Consumer electronics, transportation systems, medical equipment, and new smart materials all make extensive use of capacitive touch sensors. One appealing method for creating structurally integrated, mechanically protected sensing systems is to embed these sensors in a polymer matrix, such as epoxy resin. Epoxy, on the other hand, is a highly insulating dielectric that modifies response speed, signal quality, effective capacitance, and electric field distribution. In order to measure and evaluate the electrical characteristics and functional performance, the main goal of the current study is to determine the viability of an embedded capacitive sensor and a capacitive sensor with a wire loop implanted beneath the epoxy surface. Epoxy-embedded capacitive touch sensors offer a potential technique for creating compact, long-lasting, and dependable sensing systems for sophisticated smart electronic applications. Their superior insulation, mechanical stability, and environmental resilience make them ideal for use in flexible electronics, HMI (human-machine interfaces), wearable sensors, and SHM (structural health monitoring) applications. However, more research is needed to determine how embedded sensor layout affects sensitivity, signal quality, and long-term performance. In order to determine their electrical and functional performance for application-specific smart sensing technologies, this study assesses two distinct novel epoxy-embedded capacitive sensor configurations.

2. Experimental Procedure

2.1. Materials and Methods

The electrically conducting protective material consisted of a commercially available epoxy resin (bisphenol-A) and the appropriate amine hardener. The epoxy material was chosen because of its excellent mechanical properties, moderate shrinkage, and exceptional electrical insulating capabilities. According to the manufacturer, the resin-to-hardener mixing ratio was kept at 10:1 by weight. To prevent an air gap and achieve homogeneity, the epoxy was gently stirred before casting. Sensor placement was carried out immediately after degassing in order to ensure appropriate positioning and insertion in the epoxy matrix. Before testing, the specimens were cured for 24 hours at room temperature (25 ± 2 °C) with a relative humidity of roughly 50 ± 5%. This was followed by another 24 hours of stabilization. Two sensor configurations were developed and shown in Figure 2:

Type A Sensor: A thin, insulated copper lead wire connects a flat, 15 mm by 15 mm copper contact electrode. In order to allow for finger contact, the electrode surface was positioned 2 mm inside the epoxy's upper surface.

Type B Sensor: A conductive copper wire loop is completely implanted in the epoxy layer. In comparison with Type A, the epoxy served as a dielectric barrier that affected the dispersion of the capacitance field rather than the sensing element, making direct contact with the surface.

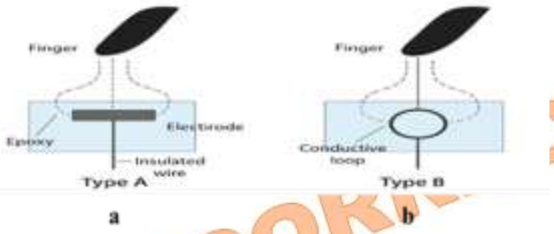

Fig. 2. Two types of sensors: a) Embedded touch sensor, b) Circular wire loop

2.2. Fabrication

Samples measuring 80 mm × 80 mm × 5 mm were cast using silicone rubber molds. To reduce contamination during preparation, extra supplies included an ultrasonic degassing chamber, a digital weighing scale, and stirring rods coated in Teflon. For the fabrication of a composite, an epoxy matrix is mixed with a hardener at a 10:1 weight ratio, and the mixture is stirred to remove the trapped air bubbles. Two different configurations are fabricated by placing the touch sensor within the epoxy matrix. For the Type-A configuration, a touch sensor is embedded with epoxy (2 mm below the top surface of the mold), and for the Type-B configuration, a sensor is placed similarly to Type A, but a semicircular loop of wire is encased throughout the epoxy as an extra arrangement. To reduce the cavities between the sensor, the mixture is poured into the mould slowly. The specimens were cured for 24hours at RT (room temperature) to increase dielectric accuracy. The present study carefully evaluates both configurations to determine the composite's electrical properties and functionality.

Both configurations use a capacitive touch sensor (TTP223) having three outputs, such as VCC (positive power supply voltage), ground, and Input/output as shown in Figures 3 (a) and (b). For the Type A configuration, the battery's positive terminal is directly linked to the LED bulb, and the negative side is connected to the ground. The VCC is connected to the wire perpendicularly, while the I/O is directly attached to the opposite side of the LED bulb.

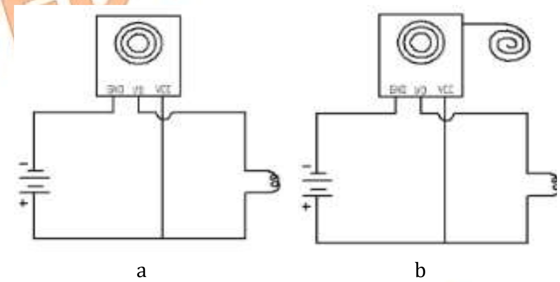

Fig. 3. Types of Circuit, a) Type A, b) Type B

2.3. Testing

The epoxy-embedded touch sensor smart

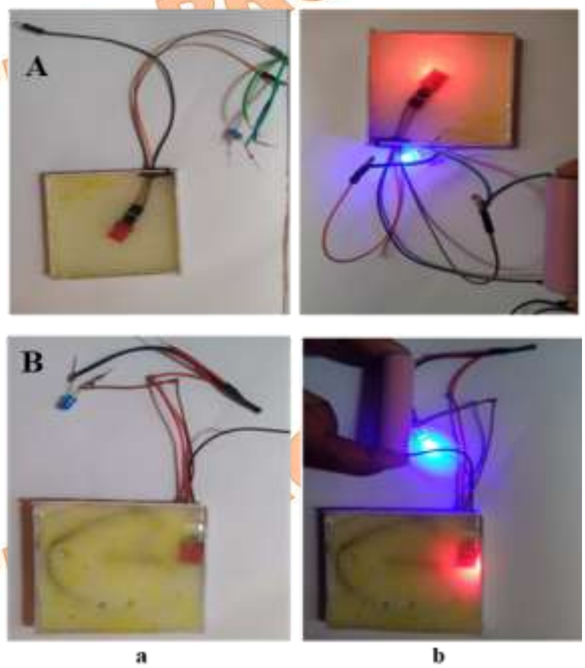

composite was successfully fabricated and tested using two different circuit configurations to evaluate electrical and functional performance under different design scenarios. The feasibility of embedding touch-sensitive electrical parts within an insulating matrix of polymers without affecting performance is shown in Figure 4. Despite being fully embedded in the epoxy resin, the sensor retained full capability in both configurations.

Fig. 4. Type A and Type B (a): Sensor and Circuit, b) LED Glow Condition with Battery.

The manufactured sensor element is integrated with a basic electrical circuit in Type A and Type B configurations, as shown in Figure 4 (a). Insulated copper wires are used to link the sensor, which is embedded in the epoxy matrix. The sensor element, a current-limiting resistor, connecting wires, and terminals for an external power supply make up the circuit. The LED is in the OFF position, and the sensor is inactive under normal (no excitation) conditions, indicating that there is either no signal or inadequate output from the sensor. The fundamental circuit architecture is needed for detecting a change in sensor response. Similarly, Figure 4 (b) represents the circuit's operating condition when linked to a battery. When the sensor is activated (by an applied stimulus such as contact, pressure, or environmental change), the electrical signal is sufficient to forward-bias the LED. Therefore, effective sensing and signal transfer across the circuit are shown by the LED glowing. A clear indication of sensor efficiency and proper circuit functioning is the glowing LED. The forward voltage drop and operating current of the LED have not been taken into account in the quantitative study of capacitance, dielectric characteristics, response time, hysteresis, or SNR characterizations, nor was it utilized as a sensing element. Irrespective of the LED characteristics, all electrical and functional performance parameters were taken directly through the sensor output and measuring tools. Thus, rather than the LED architecture, the observed variations between Type A and Type B correspond to the sensor geometry and electrode configuration.

2.4. Functional Performance and Electrical Characterization

Resistivity, capacitance, dielectric, and other methods of testing are used to evaluate electrical properties. Conductivity and resistivity were measured using a digital LCR meter that operated at a steady frequency of 1 kHz. Using Eq. 1.

$$\rho = RA/L \qquad (1)$$

where ρ = resistivity (ρ), R = measured resistance, A = effective electrode area (15 mm × 15 mm), and L = thickness of the epoxy layer between the electrodes. The study provided insight into whether the embedded electrode or loop structure affected the charge transport behavior in the epoxy matrix. A frequency range of 100 Hz to 1 MHz was used to test the dielectric and capacitive characteristics. This test permitted the examination of the epoxy-embedded sensor system's frequency-dependent permittivity. The touch-triggered capacitance variation (ΔC) was measured by a finger on or close to the sensor surface. Both configurations of variations in capacitance showed touch sensitivity and effective electric-field penetration through the epoxy matrix.

Sensitivity, response time, SNR (signal-to-noise ratio), and repeatability tests were used to evaluate the functional performance of both configurations. Touch sensitivity was assessed by determining a variation in capacitance (ΔC) at specified finger pressure ranging from 0.1 to 0.5 N in order to find out whether the mechanical stress influences the electric-field interaction across the epoxy layer. Response time was measured using a digital oscilloscope, with the increase in time between 10% and 90% of the output signal amplitude providing data regarding the sensor's dynamic behavior and velocity. The SNR was determined using equation (2).

$$SNR = 20\log (V_{Signal} / V_{Noise}) \qquad (2)$$

A 100-cycle repeatable touch test was used to determine functional repeatability, and the coefficient of variation was computed. It analyzes the level of clarity and durability of the sensor's output when subjected to ambient electrical noise. This repeatability study has been used to determine the stability and long-term resilience of both configurations.

A statistical analysis using a Two-Sample t-Test was used to compare Type A and Type B sensors. Error bars were used to analyze measurement deviation, and a seven-day monitoring period was used to evaluate long-term stability. The goal of the comparison investigation was to identify the best setup for touch-sensing applications.

3. Results and Discussion

3.1. Electrical Characterization

Both configurations' electrical performance was examined in terms of conductivity and resistivity, and plain epoxy was taken into consideration as an extra reference configuration to serve as a baseline (control sample). The epoxy-sensor structure's bulk resistivity (ρ) was assessed using the four-point probing method and validated using an LCR meter under low-frequency AC and DC excitation.

Table 1. Electrical Conductivity and Resistivity

Sample	Resistivity (Ω·m) × 10^{8}	Conductivity (S/m) × 10^{-9}
Neat Epoxy	2.3	4.3
Type A	1.9	5.2
Type B	1.8	5.5

The measured electrical resistivity, along with the conductivity of two sensor configurations (Type A and Type B) and neat epoxy (control), is shown in Table 1. Neat epoxy shows an excellent resistance value of 2.3×10^{8}Ω·m and a lower conductivity value of 4.3×10^{-9} S/m, which indicates better insulating properties compared to its counterparts. These properties of neat epoxy act as a reference point for analysing the sensor-embedded composites' electrical behaviour. In a Type A configuration, the resistivity is 1.9×10^{8} Ω·m and the conductivity is 5.2×10^{-9} S/m. These values show a decrease compared to the reference point, which indicates the development of an additional pathway within epoxy, which may be a result of enhanced movement of electrons. The small shift validates the epoxy-sensor system's sensitivity to electrical stimulation. Similarly, the Type B configuration shows the resistivity is 1.8×10^{8} Ω·m and the conductivity is 5.5×10^{-9} S/m. High conductivity and low resistivity indicate an improved electrical pathway, higher sensing spread, and a higher level of electrical phase consistency. The incremental reduction in resistivity from Type B to pure epoxy effectively demonstrates how sensor layout improves electrical performance.

3.2. Dielectric and Capacitance Behavior

The frequency-dependent capacitance and dielectric behavior of both configurations are shown in Table 2. Epoxy matrix-based dielectric systems.

Table 2. Frequency-Dependent Dielectric Constant and Capacitance Variation

Frequency (Hz)	εr (Type A)	εr (Type B)	ΔC (pF) under touch
100	3.8	4.1	14.6
1k	3.5	3.8	12.2
10k	3.3	3.6	9.1
100k	3.1	3.3	7.8

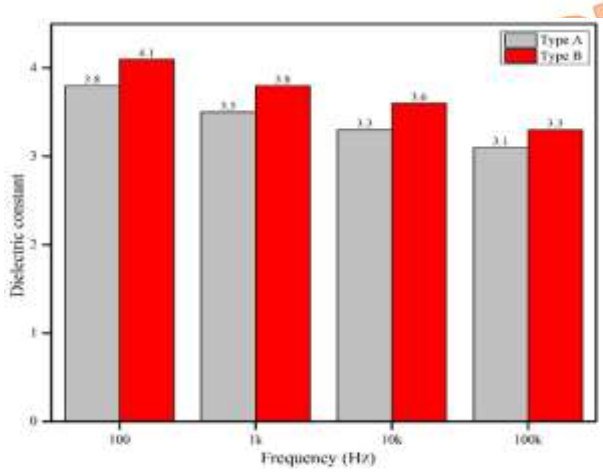

Fig. 5. Frequency-dependent dielectric behaviour

Figure 5 indicates that the dielectric constants (εr) of both configurations show a decrease in values as the frequency increases from 100 Hz to 100 kHz. A higher dielectric constant value for both configurations, 3.8 and 4.1, was obtained at 100Hz. This phenomenon may be due to the dipolar, polarized orientation and interfacial mechanics that interact to integrate the carriers of charges and dipoles with the induced electric field. The effects of Maxwell-Wagner-Sillars (MWS) polarization at the epoxy/metal interface, in which wires and embedded electrodes facilitate charge generation, as well as dipolar polarization within the epoxy matrix, are responsible for the higher dielectric constant seen in both configurations at lower frequencies. The dielectric constant gradually decreases as the frequency rises because polar molecule groups and interfacial charges are less able to follow the quickly switching electric field. For each frequency interval, Type B dielectric constant values are increasingly higher than Type A, suggesting better polarization capacity. This can be caused by better interface contact, better sensor design, or more effective permittivity within the sensor layer. An identical frequency-dependent pattern is observed in the ΔC (touch-induced capacitance variation), which reduces from 14.6 to 7.8 pF at 100 Hz and 100 kHz. Higher capacitive sensitivity and charge storage at low frequencies are indicated by larger ΔC. On the other hand, constrained charge transfer, characterized by a lower surface polarization influence at low frequencies, is indicated by a lower ΔC. In conclusion, it is observed that both dielectric performance and capacitive sensitivity are highly frequency dependent, with the Type B configuration showing enhanced touch sensitivity and enhanced dielectric performance at lower frequencies.

Dielectric relaxation linked to dipolar and interfacial polarization mechanisms is the main cause of the dielectric constant's reduction with increasing frequency. Polar groups in the cross-linked epoxy matrix and charge accumulation at the epoxy–sensor interfaces can efficiently align with the applied electric field at lower frequencies (100 Hz–1 kHz), leading to greater dielectric constant values. Dipoles and interfacial charges are less able to react as the frequency rises because the electric field changes direction more quickly. As a result, they contribute less to the total polarization, which causes the dielectric constant to drop over the studied frequency range from 3.8 to 3.1 for Type A and from 4.1 to 3.3 for Type B. Only the quicker electronic and atomic polarization mechanisms are effective at higher frequencies, and they make up a smaller portion of the total permittivity. This result is in line with the Debye dielectric relaxation hypothesis, which states that when the applied frequency surpasses the dipolar species' capacity for relaxation, the dielectric constant falls. The current investigation didn't utilize high-level dielectric spectroscopy to determine intrinsic epoxy relaxation and interfacial polarization impacts separately; the dielectric properties of the neat epoxy reference, as well as the frequency-dependent characteristics of both sensor configurations, suggest that both mechanisms influence the overall response. The higher dielectric constant of Type B is most likely connected with increased interfacial polarization due to the increased electrode-polymer interaction area offered by the circular wire loop design. As a result, the dielectric response is thought to be caused by both intrinsic dipolar relaxation and extrinsic charge accumulation at polymer-metal contacts.

3.3. Functional Testing of Embedded Touch Sensors

Both configurations are tested for functionality to examine the ability to detect touch and proximity behaviour. The factors that are assessed include repeatability, touch sensitivity, response time, and SNR. The variation in capacitance under applied touch force for both configurations is shown in Figure 6.

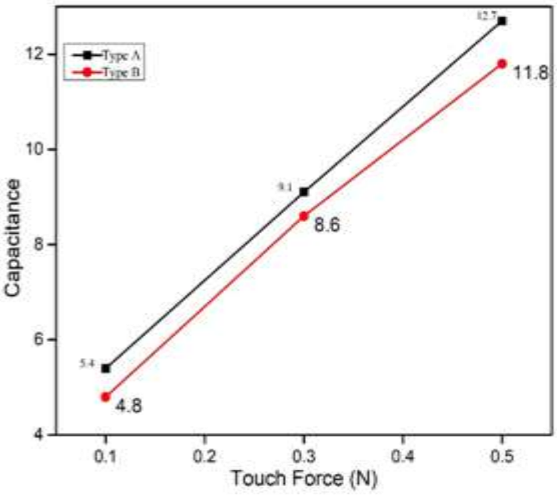

Fig. 6. Touch Force Vs Capacitance

As observed in Figure 6, Type A and Type B configurations exhibit a stable and repeatable capacitance response within the applied force range of 0.1–2 N. At lower forces (0.1–0.5 N), both sensors demonstrate high sensitivity, indicating their capability to detect light touch interactions. With further increase in force up to 2 N, the capacitance response continues to increase, confirming the ability of the sensors to distinguish different levels of applied pressure. Since a typical human touch force is approximately 1 N, the obtained response within this range demonstrates the suitability of the developed sensors for touch interfaces, wearable electronics, and human–machine interaction applications. Capacitance values of 5.4 and 4.8 pF are shown for Type A and Type B configurations at 0.1 N. At 0.3 N, the capacitance values increase from 9.1 to 8.6. Similarly, at 0.5 N, capacitance values increase from 12.7 to 11.8 pF. Increase in capacitance across all touch forces for both configurations. For Type A, the increase may be due to the enhanced effective dielectric constant and elasticity. The linear trend in the graph shows the excellent consistency and appropriate response time for both configurations. Because the electrodes are nearer the surface, Type A has better interaction with the body's capacitance and is therefore more sensitive, making it suitable for touch sensing in reliable touch-sensing applications. Type B is appropriate for applications requiring waterproofing or insulation because of its softer, more dependable behavior curves.

An oscilloscope was used to determine the transient performance of the sensors in order to investigate their reaction time characteristics. Table 3 illustrates the observed fluctuation (rise and fall) in times. For testing of a touch-sensitive application, the delay of 20 to 30 ms (total delay can be less than 100ms) is acceptable. In the fluctuation, the fall time is the amount of time it takes for the signal to fall back to its baseline following touch release, while the rise time is the amount of time it takes for the sensor output to react to touch detection. With a rise time of 45 ms and a fall time of 50 ms, the Type A configuration reacts more quickly, indicating quick charge accumulation and discharge in the sensor layer. It is also found to have superior dynamic performance due to its faster detection and response time, making it more suitable for applications that require fast reactions to frequently occurring touch signals. Type B configurations also show a similar trend with a rise time of 65ms and a fall time of 72 ms, which displays weaker dynamics. More gradual charge redistribution across the sensor layer, higher resistance within the layer, or improved dielectric relaxation could be reasons for Type B's longer response times.

Table 3. Response Time Characteristics of Type A and Type B Sensor Configurations

Configurations	Rise Time (ms)	Fall Time (ms)
Type A	45	50
Type B	65	72

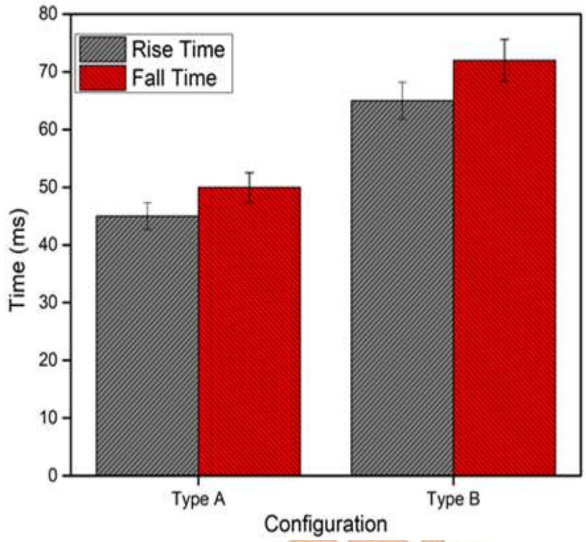

Fig. 7. Comparison of rise time and fall time for Type A and Type B sensor configurations.

Figure 7 shows that the relatively low standard deviations indicate high measurement repeatability and sensor stability. Type A's faster reaction can be attributed to lesser electrical damping and higher touch sensitivity, whereas Type B's longer response time is due to improved insulation and dielectric damping characteristics induced by the encapsulation configuration.

The SNR performance of the sensors was determined by comparing the variation in average voltage under touch (signal) and no-touch (noise) conditions, as shown in Table 4. Considering a peak-to-peak signal voltage, the Type A configuration obtained an SNR of 30.8 dB (a noise level of 0.11 Vrms and 3.8 Vpp). This indicates an effective output signal, but because of the relatively higher noise level, the overall SNR is significantly reduced. Type B, on the other hand, has a much lower noise level of 0.08 Vrms but a relatively lower signal amplitude of 3.5 Vpp, resulting in a higher SNR of 32.8 dB. Enhanced noise reduction and signal stability are suggested by Type B's higher SNR, which is probably the result of superior electrode configuration, increased dielectric consistency, or fewer parasitic influences. Type B delivers better signal clarity and dependability, which is essential for accurate touch detection and reducing false triggering, even though Type A gives a bigger absolute signal magnitude. The results indicate that, to achieve greater SNR for capacitive touch sensor performance, effective noise reduction is more important than signal amplitude. Because of the epoxy's ability to filter out ambient noise, Type B has a slightly higher SNR. This demonstrates that by protecting against external electromagnetic interference (EMI), epoxy encapsulation increases stability.

Table 4. Signal-to-Noise Ratio (SNR) Performance of Type A and Type B Sensor Configurations

Condition	Signal (Vpp)	Noise (Vrms)	SNR (dB)
Type A	3.8	0.11	30.8
Type B	3.5	0.08	32.8

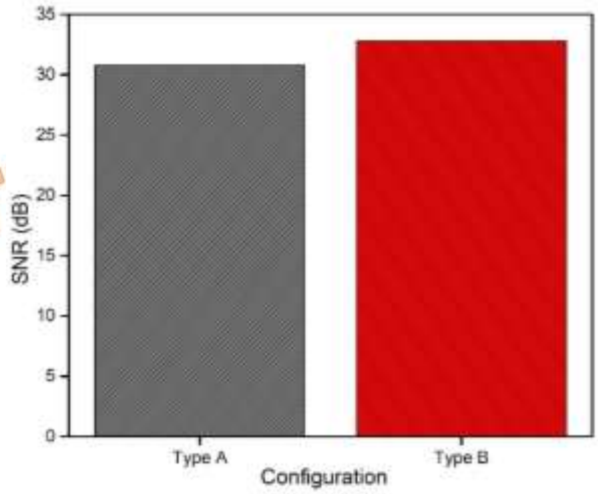

Fig. 8. Comparison of signal-to-noise ratio (SNR) between Type A and Type B sensor configurations.

Figure 8 shows a comparison of the signal-to-noise ratio (SNR) between Type A and Type B sensor configurations. Type B indicates better measurement consistency and electrical stability. The greater SNR of Type B can be due to the encapsulation structure's improved insulation and dielectric damping, which eliminates unexpected electrical fluctuations and enhances the quality of the signal. Both configurations have reasonably modest error bars, confirming the sensor output's repeatability and dependability during repeated touch readings.

The sensor functionality performance tests were carried out using repeatability and hysteresis tests. Repeatability tests were conducted under ambient laboratory conditions (at Room temperature (25±2°C) and (50±5%) relative humidity). A force-controlled arrangement was used to apply a continuous touch force of 2.5N at a loading rate of 2N/s. 100 consecutive touch-release cycles were used to determine repeatability and hysteresis. Before the next cycle, each touch event was sustained for about 1 second, after which there was a one-second release time. During the loading (touch) and unloading (release) phases, capacitance responses were constantly monitored. The consistency of capacitance fluctuation across multiple cycles was used to evaluate repeatability, and the most significant variation within the loading and unloading outputs calculated by the full-scale capacitance output was used to compute hysteresis error. The repeatability percentage was determined using equation (3)

$$Repeatability\ (\%) = (1 - CV) \times 100 \quad (3)$$

where CV is the ratio of the standard deviation to the mean capacitance response. A lower coefficient of variation corresponds to higher repeatability and measurement consistency.

The test was carried out for 100 touch release cycles in succession, and the results are displayed in Figure 9. Capacitance repeatability is the repeatability of the output of sensors within the same loading conditions across multiple cycles. Type A has excellent consistency with relatively minimal variation cycle-to-cycle, with a repeatability of 96.7%. Whereas Type B shows an enhanced repeatability of 98.2%, indicating improved consistency and a more consistent capacitance response across repeated cycles.

The hysteresis error is the difference in sensor output between the loading and unloading cycles with identical applied touch force. The percentage hysteresis error (HE%) is determined using Equation (4).

$$HE\ \% = \left({}^{\Delta V_{max}}/_{V_{FS}}\right) \times 100 \quad (4)$$

where ΔVmax is the maximum difference between the output voltage values obtained during the loading and unloading paths at the same input condition, and V_{FS} is the full-scale output voltage range of the sensor. Type A configuration hysteresis error is 2.1%, which indicates a significant loss of energy or a slower recovery caused by viscoelastic influences within the sensor layer. Type B configuration recovery occurs at a quicker rate and with less dielectric relaxation, with the reduced hysteresis error of 1.4%. Both the configuration with higher repeatability and with lesser hysteresis error, Type B, can be the best configuration with respect to long-term and repetitive tactile sensing. applications. The viscoelastic properties of the polymer matrix, which display both elastic deformation and time-dependent viscous relaxation, are the main reason for hysteresis in epoxy-based sensors. Hysteresis behavior is caused by the delayed recovery of polymer chains during unloading, which causes a discrepancy between loading and unloading reactions. The degree of viscoelastic relaxation and energy loss in the epoxy matrix determines the magnitude of hysteresis. Because of less stress accumulation and delayed recovery effects, Type B's hysteresis error (1.4%) is lower than Type A's (2.1%), indicating decreased viscoelastic losses and enhanced sensor stability. The increase in capacitance with applied touch force is mainly due to a decrease in the effective sensor thickness, which improves electric-field coupling. However, because epoxy is viscoelastic, time-dependent deformation mechanisms such as creep and delayed elastic recovery may affect the observed capacitance response under sustained or frequent loading conditions. An enhancement in capacitance might result from compression of the epoxy layer upon touch application, which can modify the dielectric distribution and electrode spacing. Usually, there is a slight delay between loading and unloading responses because the epoxy does not instantly recover once the load is removed; instead, it slowly recovers to its original geometry. Electrical and mechanical relaxation situations may have an impact on the measured hysteresis. While mechanical contributions come from the viscoelastic recovery of the epoxy matrix, electrical contributions come from charge redistribution, dielectric polarization, and interfacial charge relaxation within the epoxy–electrode system.

Enhanced SNR and decreased hysteresis observed in Type B may be due to the altered fringed electric field distribution produced by the circular wire loop arrangement. In Type A, a more concentrated and dispersed electric field surrounds the sensing region, reducing undesired parasitic coupling with nearby electrical sources and enhancing signal stability. The circular loop geometry increases the accumulation of charge in the dielectric region and encourages a more uniform distribution of electric fields, which improves capacitive response consistency and lowers noise contribution. The Parasitic capacitance, optimum sensing area, and electric field intensity are all influenced by the loop geometry parameters (number of circular loops, wire, and loop diameter). As the diameter of the loop increases, the sensitivity and area of interaction also increase, but excessive dimensions might enhance fringe-field exposure and parasitic effects. The number of loops can alter capacitive coupling and effective inductive properties, while wire gauge affects charge transfer capacity and electrode resistance. A single circular wire loop topology was chosen for the current investigation in order to strike a balance between signal stability, fabrication ease, and sensing sensitivity. Therefore, the optimal electric field confinement, decreased ambient interference, and stable charge redistribution made possible by the loop electrode configuration are linked to the enhanced SNR and decreased hysteresis of Type B.

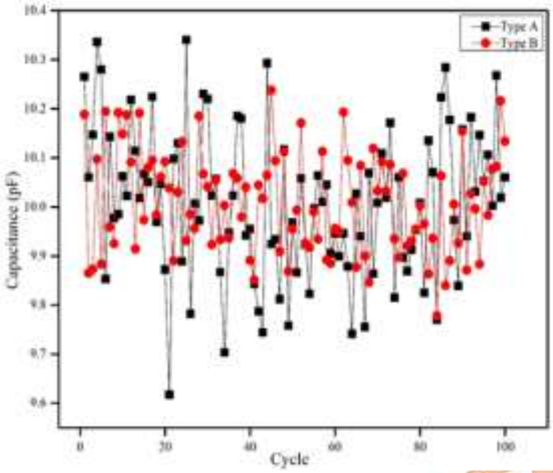

Fig. 9. Repeatability performance of Type A and Type B epoxy-embedded capacitive sensor configurations over 100 touch cycles.

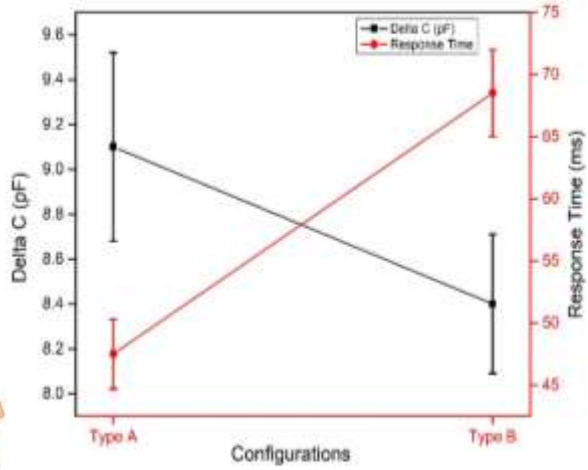

Fig. 10. Comparison of mean touch-induced capacitance variation (ΔC) and response time for Type A and Type B sensor configurations

3.4. Statistical Analysis using Two-Sample t-Test and Error Estimation

Both configurations are tested statistically by performing a two-sample t-test by comparing the response time and variation of capacitance (ΔC) induced by touch. The test was carried out with a confidence level of 95% (critical value less than 0.05). The variation in capacitance had a mean value of 9.1 pF and 8.4 pF for Type A and Type B configurations, respectively. Both configurations perform significantly, with a critical value of 0.032, which is less than 0.05. Type A configuration enhanced touch sensitivity can be observed through its better variation in capacitance under similar touch conditions. Similarly, for response time, the critical value is 0.018, and the mean values are 47.5 and 68.5 for Type A and Type B configurations, respectively. Type A would be ideal for faster response times and enhanced sensitivity. Type B is more stable in changing environmental conditions due to its longer response time and better signal stability, which is associated with improved electrical resistance and noise reduction. This statistical analysis confirms that both configurations indicate a clear correlation between resilience and sensitivity, and they differ functionally.

Table 5. Statistically significant differences between the two configurations

Metric	Type A Mean	Type B Mean	p-value	Significance
ΔC (pF)	9.1	8.4	0.032	Significant
Response Time (ms)	47.5	68.5	0.018	Significant

Figure 10 shows that the minimal standard deviations suggest high measurement accuracy and repeatability. A two-sample t-test indicated statistically significant variations in ΔC ($p = 0.032$) and response time ($p = 0.018$) between the two sensor setups, indicating distinct sensing capabilities.

Error estimation is carried out for the above with the Standard deviation (σ) and coefficient of variation (CV) for the capacitance and response time variables, which were used to assess the measurement error of the touch sensor system. Repeatability over multiple touches and a modest level of variation between the average, as indicated by capacitance readings, with SD (standard deviation) 0.42 and 4.6% CV. Similarly, for response time, 2.8ms SD and 5.2% CV are observed, displaying consistent dynamic characteristics with limited variation over time. The error limits for both factors remain within ±5% for functional touch sensing and interface between humans and machine applications, where small variations do not affect performance or customer behavior. The relatively low CV values indicate stable performance of the sensor and steady processing of signals. In addition, by reducing multiple touch mechanical disturbances, high-frequency electrical variations, and external interference, the sensing device's protective cover contributes significantly to data accuracy.

Three samples ($n = 3$) from each sensor configuration were tested, and the average capacitance value was considered for evaluating long-term stability. The samples were stored at room temperature (25 ± 2°C) and relative humidity (50 ± 5%), and they were placed away from direct sunlight exposure to prevent environmental degradation for 60 days. At regular intervals (10days), each sensor configuration had 3 samples examined, and the mean capacitance value was taken into account to determine long-term stability. Capacitance values reduced from 25 to 24.5 pF and 23.5 to 23.4 pF for Type A and Type B configurations, respectively. Type A capacitance values decreased by 2%, and the Type B configuration shows more stability, maintaining nearly constant capacitance values. Both configurations show a reduction in performance over the time period; these reductions are negligible, and they are within the limit and show good agreement with long-term performance, making them ideal for long-term practical performance that does not require regular maintenance. This long-term resistance to degradation is caused by the excellent shielding properties of the epoxy, which effectively stop moisture absorption and the oxidation of conductive channels. Through this shielding, the sensor and wiring parts are protected from environmental changes and also protect electrode durability and dielectric consistency.

4. Conclusions

The current study used epoxy with an embedded capacitive touch sensor for fabrication. The integration of capacitive touch sensors within an epoxy matrix using two distinct configurations: Type A (embedded sensor) and Type B (embedded sensor with circular wire loop). Both configurations are tested for electrical and functional characteristics. The fabricated structures maintained full sensing functionality after encapsulation, confirming the feasibility of embedding capacitive sensing elements within electrically insulating polymer matrices without compromising operational performance. The significant results and conclusions are as follows:

- Electrical characterization confirmed that both configurations retained the intrinsic insulating behavior of the epoxy matrix while providing effective capacitive sensing performance, indicating their suitability for embedded sensing applications.
- The dielectric constants of both configurations, which show a decrease in values as the frequency increases from 100 Hz to 100 kHz. A higher dielectric constant value for both configurations, 3.8 and 4.1, was obtained at 100Hz. Dielectric analysis revealed frequency-dependent behavior over the investigated frequency range, with Type B exhibiting comparatively higher dielectric permittivity, suggesting enhanced polarization capability and charge-storage characteristics.
- The Capacitance variation reduces from 14.6 to 7.8 pF at 100 Hz and 100 kHz. Higher capacitive sensitivity and charge storage at low frequencies are indicated by larger ΔC. On the other hand, constrained charge transfer with a lower surface polarization influence at low frequencies is indicated by lower ΔC.
- The ability of both configurations to detect forces within the 0.1–2 N range confirms their suitability for low-pressure sensing applications. Capacitance values of 5.4 and 4.8 pF are shown for Type A and Type B configurations at 0.1 N. Similarly, at 0.5 N, capacitance values increase from 12.7 to 11.8 pF. Increase in capacitance across all touch forces for both configurations. For Type A, the increase may be due to the enhanced effective dielectric constant and elasticity. Type B is appropriate for applications requiring waterproofing or insulation because of its softer, more dependable behavior curves.
- Functional performance showed that Type A provided higher sensitivity and faster response characteristics, whereas Type B exhibited superior SNR, lower hysteresis, improved repeatability, and enhanced resistance to electrical noise. Statistical analysis confirmed a significant difference in capacitance response and transient behavior between the two configurations ($p < 0.05$), highlighting the influence of sensor architecture on overall performance.
- Long-term aging test (samples tested for 60days for different time intervals) was observed with excellent environmental stability and durability, which shows less than 2% capacitance degradation and hysteresis error; repeatability tests showed minimal variation, less than 6%.

Both configurations performed well in terms of electrical and functional performance. The Type A configuration shows enhanced sensitivity and quicker response time, and should be considered for applications that require fast detection of signals, including touch interfaces, interactive flexible electronics, and HMI (human-machine interface) systems. Type B configuration shows excellent electrical performance, long-term durability, and noise rejection, and is better suited for applications that require increased reliability in different kinds of environments, such as SHM (structural health monitoring), wearable sensors, and flexible electronic systems that can operate for extended periods of time. The obtained results present a solid basis for material selection and adaptation of epoxy matrix-embedded capacitance touch sensor structures for particular applications in man-machine interface and smart sensor technologies.

Funding Statement

This research did not receive any specific grant from funding agencies in the public, commercial, or not-for-profit sectors.

Conflicts of Interest

The author declares that there is no conflict of interest regarding the publication of this article.

References

[1] T. S. Mohan Kumar, Sharnappa Joladarashi, S. M. Kulkarni, Saleemsab Doddamani, "Optimization of process parameters for ballistic impact response of hybrid sandwich composites", International Journal on Interactive Design and Manufacturing (IJIDeM), Volume 17, pages 1099–1111, (2023), https://doi.org/10.1007/s12008-022-01061-2.

[2] Meng Wang, Gongdong Wang, Mingyang Zheng, Chengyang Xu, Zhendong Liu, Yuxuan Yang, "Epoxy resin reinforced high-performance conductive composite foam with ultra-wide pressure sensing range", Electrochimica Acta, Volume 484, 20 April 2024, 144109, https://doi.org/10.1016/j.electacta.2024.144109.

[3] Chuan Wang, David Hwang, Zhibin Yu, Kuniharu Takei, Junwoo Park, Teresa Chen, Biwu Ma, and Ali Javey "User-interactive electronic skin for instantaneous pressure visualization," Nature Mater., Letters, Published Online: 21 July 2013 vol. 12, no. 10, pp. 899–904, Oct. 2013, DOI: 10.1038/NMAT3711.

[4] Dae-Hyeong Kim, Nanshu Lu, Rui Ma, Yun-Soung Kim, Rak-Hwan Kim, Shuodao Wang, Jian Wu, Sang Min Won, Hu Tao, Ahmad Islam, Ki Jun Yu, Tae-il Kim, Raeed Chowdhury, Ming Ying, Lizhi Xu, Ming Li, Hyun-Joong Chung, Hohyun Keum, Martin McCormick, Ping Liu, Yong-Wei Zhang, Fio-renzo G. Omenetto, Yonggang Huang, Todd Coleman, John A. Rogers, "Epidermal electronics," Science, vol. 333, pp. 838–843, 2011, DOI:10.1126/science.1206157.

[5] P. Drzaic, B. Comiskey, J. D. Albert, L. Zhang, A. Loxley, R. Feeney, J. Jacobson, "44.3L: A printed and Rollable Bistable electronic display," Int. Symp. Dig. Tech. Papers, vol. 29, no. 1, 1998, Art. no. 1131, https://doi.org/10.1889/1.1833686.

[6] G. Walker, "A review of technologies for sensing contact location on the surface of a display: Review of touch technologies," J. Soc. Inf. Display, vol. 20, no. 8, pp. 413–440, Aug. 2012.

[7] Z. Zhao, K. Liu, Y. Liu, Y. Guo, and Y. Liu, "Intrinsically flexible displays: Key materials and devices," Nat. Sci. Rev., vol. 9, no. 6, Jun. 2022, Art. no. nwac090.

[8] Y.-S. Jang, K.-U. Gwak, S.-S. Lee, S.-G. Lee, J.-H. Kim, and H.-S. Oh, "P-181: A charge- share-based relative read-out circuit for capacitance sensing," Int. Symp. Dig. Tech. Papers, vol. 41, no. 1, pp. 1937–1939, 2010.

[9] K. Kyoung, K. Yuge, and R. Hattori, "Single-layered and one-sided wired capacitive touch panel using transient electrical response," in Proc. 18th Int. Display Workshops, 2011, pp. 1341–1344.

[10] Padmam Gopinath Kaimal, "Review on Recent Advances on Touch Sensor for Flexible Displays", International Journal of Trend in Scientific Research and Development (IJTSRD), Volume 8, Issue 6, 941-950, Nov-Dec 2024. Available Online: www.ijtsrd.com e-ISSN: 2456 – 6470.

[11] G. Barrett and R. Omote, "Projected-capacitive touch technology," J. Inf. Display, vol. 26, no. 3, pp. 16–21, Mar. 2010.

[12] J.-Y. Ruan, P. C.-P. Chao, and W.-D. Chen, "A multi-touch interface circuit for a large-sized capacitive touch panel," in Proc. IEEE Sensors, 2010, pp. 309–314.

[13] Y. Ling, T. An, L.W. Yap, B. Zhu, S. Gong, W. Cheng, "Disruptive, soft, wearable sensors", Advanced Materials, 32 (2020), Article e1904664, 10.1002/adma.. 201904664.

[14] B. Dong, Y. Yang, Q. Shi, S. Xu, Z. Sun, S. Zhu, Z. Zhang, D.L. Kwong, G. Zhou, K.W. Ang, C. Lee, "Wearable triboe-lectric-human-machine interface (THMI) using robust nano-photonic readout", ACS Nano, 14 (2020), pp. 8915-8930, 10.1021/acsnano 0c03728.

[15] Zhuyu Ma, Yang Zhang, Kaiyi Zhang, Hua Deng, Qiang Fu, "Recent progress in flexible capacitive sensors: Structures and properties", Nano Materials Science, Volume 5, Issue 3, September 2023, Pages 265-277, https://doi.org/10.1016/j.nanoms.2021.11.002.

[16] Muh. Supwatul Hakim, Muhammad Roil Bilad, "Colorimetric Sensor for Heavy Metal Ions Detection: A Short Review", EVERGREEN Joint Journal of Novel Carbon Resource Sciences & Green Asia Strategy, Vol. 11, Issue 04, pp3127-3142, December, 2024.

[17] Vikas Singh Panwar, Imran Moujan, Aman Kazi, Pratik Kale, Satyam Rode, Anish Pandey, Shyam Mogal, "A Review on Design and Characteristics of Landmine Detection

Robot", EVERGREEN Joint Journal of Novel Carbon Resource Sciences & Green Asia Strategy, Vol. 11, Issue 02, pp. 900-912, June, 2024

[18] N. Luo, W. Dai, C. Li, Z. Zhou, L. Lu, C.C.Y. Poon, S.-C. Chen, Y. Zhang, N. Zhao, " Flexible piezoresistive sensor patch enabling ultralow power cuffless blood pressure measurement", Adv. Funct. Mater, 26 (2016), pp. 1178-1187, 10.1002/adfm. 201504560.

[19] H. Kim, G. Kim, T. Kim, S. Lee, D. Kang, M.S. Hwang, Y. Chae, S. Kang, H. Lee, H.G. Park, W. Shim, "Transparent, flexible, conformal capacitive pressure sensors with nano-particles", Small, 14 (2018), 10.1002/smll. 201703432.

[20] V. Kumar, A. Kumar, S.S. Han, S.-S. Park, "RTV silicone rubber composites reinforced with carbon nanotubes, titanium dioxide and their hybrid: mechanical and piezoelectric actuation performance", Nano Mater. Sci. (2020), 10.1016/j.nanoms.2020.12.002.

[21] W. Chen, X. Yan, "Progress in achieving high-performance piezoresistive and capacitive flexible pressure sensors: a review", J. Mater. Sci. Technol., 43 (2020), pp. 175-188, 10.1016/j.jmst.2019.11.010.

[22] Arpit Srivastava1, Sanjeev Kumar Singh Yadav, "Multi-Objective Optimization of Milling ECSM Process Through PCA-Based GRA", EVERGREEN Joint Journal of Novel Carbon Resource Sciences & Green Asia Strategy, Vol. 10, Issue 04, pp2230-2236, December 2023.

[23] S. Wang, K. Shi, B. Chai, S. Qiao, Z. Huang, P. Jiang, X. Huang, "Core-shell structured silk Fibroin/PVDF piezoelectric nanofibers for energy harvesting and self-powered sensing", Nano Mater. Sci. (2021), 10.1016/j.nanoms.2021.07.008.

[24] Mehdi Mohammadimehr, "The effect of a nonlocal stress-strain elasticity theory on the vibration analysis of Timoshenko sandwich beam theory", Advances in Nano Research, Volume 17, Number 3, September 2024, pages 275-284, DOI: https://doi.org/10.12989/anr.2024.17.3.275.

[25] Behnam Mokhtarian Dehkordi, Mehdi Mohammadimehr, "Forced Vibration Response of a Sandwich Cantilever Nine-Layer Microbeam with Homogeneous Core Reinforced by Nanocomposite and Piezo-Magneto-Electric Layers as a Self-Sensing Mass Sensor",

[26] Shima Mohammadian, Mehdi Mohammadimehr, Mohsen Irani-Rahaghi & Fatemeh Bargozini, "Deflection and buckling of a sandwich curve beam with variable cross-section using fifth-order shear deformation theory with FEM: a piezoelectric layer, hierarchical and conventional honeycomb core", Mechanics Based Design of Structures and Machines, 2026, VOL. 54, NO. 1, 1–26, https://doi.org/10.1080/15397734.2026.2614989

[27] P. Nikbakhsh, M. Mohammadimehr & F. Bargozini, "Vibration of a Sandwich Plate with FG Porous and Auxetic Cores and Piezo-Electro-Magnetic Face Sheets", ISSN 1029-9599, Physical Mesomechanics, 2025, Vol. 28, No. 6, pp. 851-869.

[28] Mohammadjavad Jafari and Mehdi Mohammadimehr, "Active control for higher-order micro sandwich beam with various cores integrated by piezoelectric layers based on MSGT on the Pasternak foundation", Journal of Vibration and Control, Journal of Vibration and Control, Volume 31, Issue 23-24, https://doi.org/10.1177/10775463241291126.

[29] H. Rocha, C. Semprimoschnig, J.P. Nunes, "Sensors for process and structural health monitoring of aerospace composites: a review", Engineering Structures, 237 (2021). https://doi.org/10.1016/j.engstruct.2021.112231.

[30] Qingqing Wang, Yuan Tian, Anchalee Duongthipthewa, Jingzheng Zhang, Menglong Liu, Zhongqing Su, Limin Zhou, "An embedded non-intrusive graphene/epoxy broadband nanocomposite sensor co-cured with GFRP for in situ structural health monitoring", Composites Science and Technology, Volume 236, 3 May 2023, 109995, https://doi.org/10.1016/j.compscitech.2023.109995.

[31] C. Tuloup, W. Harizi, Z. Aboura, Y. Meyer, K. Khellil, R. Lachat, "On the use of in-situ piezoelectric sensors for the manufacturing and structural health monitoring of polymer-matrix composites: a literature review", Composite Structures, 215 (2019), pp. 127-149, https://doi.org/10.1016/j.compstruct.2019.02.046.